PCCP

PAPER

View Article Online
View Journal | View Issue

Cite this: *Phys. Chem. Chem. Phys.*, 2018, **20**, 16847

$CsPbBr_3$ and $CH_3NH_3PbBr_3$ promote visible-light photo-reactivity†

Shankar Harisingh,[a] Sujith Ramakrishnan,[a] Michael Kulbak,[b] Igal Levine,[b] David Cahen,[b] Bat-El Cohen,[a] Lioz Etgar[a] and Micha Asscher*[a]

Received 23rd February 2018,
Accepted 23rd May 2018

DOI: 10.1039/c8cp01235k

rsc.li/pccp

Inorganic and organic lead halide perovskite materials attract great interest in the scientific community because of their potential for low-cost, high efficiency solar cells. In this report we add a new property of these materials, namely their photochemical activity in the visible light range. Both inorganic ($CsPbBr_3$) and organic ($CH_3NH_3PbBr_3$-$MAPbBr_3$) perovskite thin films were demonstrated to promote photo-dissociation of adsorbed ethyl chloride (EC), employing 532 nm pulsed laser irradiation under ultra-high vacuum (UHV) conditions. From the post-irradiation temperature programmed desorption (TPD) analysis, the yield of photoproduct formation was found to be up to two orders of magnitude higher than for UV light-excited EC molecules on metallic and oxide surfaces. Photo-reactivity on top of the $CsPbBr_3$ surface is almost an order of magnitude more efficient than on the $CH_3NH_3PbBr_3$ surface, apparently due to the lower density of defect and surface states. A direct correlation was found between electron-induced luminescence and photoluminescence intensities and the photoreactivity cross-sections. We conclude that both the intense luminescence and the well-known photovoltaic properties associated with these halide perovskite materials are consistent with the efficiency of photo-reactivity in the visible range, reported here for the first time.

1. Introduction

Developing a clean and renewable source of energy to reduce the reliance of our society on fossil fuels is one of the major challenges of the 21st century. Among the alternative energy sources, solar energy is particularly attractive owing to its abundance and easy accessibility. While photovoltaics (PV) is a well-developed non-biological route of quantum conversion of solar light, in this case to electrical energy, photo-catalysis, which can both convert and store solar energy, in this case into chemical energy, is still rather less efficient, in particular with visible light excitation. Over the past decades, there have been a large number of applications developed for photocatalysts, such as, water splitting for hydrogen production,[1] degradation of organic pollutants for water purification,[2] self-cleaning surfaces,[3] air purification,[4] conversion of CO_2 to hydrocarbons[5] *etc.* While many semiconductors, ternary and other complex oxide systems have been explored as photocatalysts, their solar-chemical energy conversion yield has been limited below 10%. Recently, organic and inorganic halide perovskites, with excellent optical and electronic properties, have attracted much attention as promising materials for photovoltaic applications.[6–9] Particularly, their low band gap, long carrier lifetime, reasonable charge mobilities and high absorption coefficients in the visible region enable them to also be applied beyond photovoltaics, in optoelectronic devices such as LEDs, lasers and photodetectors.[10–12] Halide perovskite-based solar cells have seen the fastest photo-electric conversion efficiency rise of any solar cell technology from $\sim$4% to $>$22% within only several years of research.[13] Photocatalytic studies that have been performed using perovskite materials were limited to oxide perovskites ($SrTiO_3$, $BaTiO_3$, $SrSnO_3$)[14–16] that do not show significant PV activity. To the best of our knowledge at present, no photochemical activity of organic and inorganic halide perovskites has been reported, possibly because of stability issues in ambient environmental conditions. In this work we demonstrate the photochemical properties of two different inorganic ($CsPbBr_3$) and organic (CH_3NH_3PbBr) halide perovskites under visible light irradiation by monitoring ethyl chloride (EC) dissociation as the probing molecule. Since both halide perovskites are sensitive to moisture and oxygen, the photochemistry experiments were performed under ultra-high vacuum (UHV) conditions. Under a clean and well-defined UHV

[a] *Institute of Chemistry, Edmund J. Safra Campus, Givat-Ram, The Hebrew University of Jerusalem, 91904, Israel. E-mail: micha.asscher@mail.huji.ac.il*
[b] *Department of Materials and Interfaces, Weizmann Institute of Science, Rehovot 76100, Israel*

† Electronic supplementary information (ESI) available: Thermal desorption spectra of EC (mass 29) from the $MAPbBr_3/SiO_2/Si(100)$ sample, comparison of post irradiation TPD spectra of photo products, integrated TPD peaks *vs.* visible (532 nm) light excitation, photon induced luminescence spectra of $CsPbBr_3$ and $MAPbBr_3$, electron induced luminescence spectra of the $CsPbBr_3$ substrate with different EC exposure (PDF). See DOI: 10.1039/c8cp01235k

environment, with *in situ* surface inspection before and following the photo-irradiation, detection of yields of reactivity and selectivity are possible. Moreover, this study enabled us to investigate the interaction of light and electrons with the halide perovskite samples from a surface science perspective to help understand fundamental properties at the halide perovskite-vacuum interface, such as photoluminescence (PL), electron beam-induced luminescence (EBIL) and charge transfer, and how these influence photochemistry at this interface.

2. Experimental details

2.1 Perovskite substrate preparation, $CsPbBr_3$

The photochemistry studies reported here were performed with SiO_2/Si(100) as the substrate for halide perovskite deposition and EC adsorption. The $CsPbBr_3$ films (300 nm thick) were prepared on a SiO_2/Si(100) substrate using a 2-step sequential deposition technique (as described in ref. 9). 1 M $PbBr_2$ (Sigma-Aldrich) in DMF was stirred on a hot plate at 75 °C for 20 min. It was then filtered using a 0.2 μm pore size PTFE filter and immediately used. The solution was spin-coated on preheated (75 °C) substrates for 1 min at 2500 rpm and was then dried on a hot plate at 75 °C for 30 min. After drying, the substrates were dipped for 10 min in a heated (50 °C) solution of 15 mg mL^{-1} CsBr (Sigma-Aldrich) in methanol for 10 min, washed with 2-propanol, dried under a N_2 stream and annealed for 10 min at 250 °C. The XRD and SEM results of $CsPbBr_3$ are shown in the ESI,† Fig. S1.

2.2 $MAPbBr_3$

400 nm thick films were prepared in a nitrogen glove box by spin coating of 2M $MAPbBr_3$ solution on a SiO_2/Si(100) substrate at 4000 rpm for 30 s. $MAPbBr_3$ solution was prepared by dissolving an equivalent amount of MABr and $PbBr_2$ (Aldrich ≥98%) in a solution of γ-butyrolactone dimethyl sulfoxide (1 : 1). Methylammonium bromide (MABr) was synthesized by reacting methylamine (40% in methanol, TCI) with excess hydrobromic acid (48 wt% in water, Aldrich) in a round bottom flask at 0 °C for 2 hours while stirring. The solvent was removed in a rotary evaporator at 50 °C. The precipitate was washed with diethyl ether and recrystallized in ethanol absolute. The XRD and SEM results of $MAPbBr_3$ are shown in the ESI,† Fig. S2.

2.3 UHV photochemistry experiments

The photochemistry experiments described here were conducted in a previously described[17] ultra high vacuum (UHV) system at a base pressure of $\sim 2 \times 10^{-10}$ Torr. The UHV chamber is equipped with a quadrupole mass spectrometer (SRS, RGA-200) that is glass shrouded with a 5 mm orifice at its end, enabling temperature programmed desorption (TPD) spectra to be measured at 1 mm distance from the sample, thus avoiding TPD signals from surfaces other than the sample. The second harmonic of a Nd:YAG laser at 532 nm has been used as the light source at a power of 1 mJ cm^{-2} per pulse (Spectra Physics INDI 20, pulse width 6 ns, and a repetition rate of 10 Hz). The reaction scheme of the photochemical process can be written as:

$$C_2H_5Cl \xrightarrow{h\nu/e^-} C_2H_5Cl^- + C_2H_{5_{(ad)}} + Cl_{(ad)}{}^-$$

The visible light irradiation (532 nm) excites electron-hole pairs which lead to C–Cl bond cleavage *via* hot electrons, consequently EC is photo-dissociated, leading to an adsorbed ethyl radical (C_2H_5) and adsorbed Cl^- *via* a dissociative electron attachment mechanism. While some of the ethyl radicals react with adsorbed H_{ad} (from the background or further photo-dissociation of the photo-products) to produce ethane, the other fraction are retained and recombine upon sample heating to form butane (C_4H_{10}). This butane is further fragmented to Mass-41 (allyl radical) and Mass-43 (propyl radical) in the QMS ionizer during post-irradiation TPD. All the chlorine atoms that were accumulated on the perovskite surface (as determined by *in situ* Auger spectroscopy) are removed between each photochemistry cycle by Ne^+ ion sputtering. In order to study the photo-dissociation of EC, post-irradiation TPD experiments were performed by tracing the mass number of the possible photo products Mass-30 (ethane), Mass-41 (the allyl radical) and Mass-43 (the propyl radical), The surface of the sample was analyzed after each photochemistry experiment using the *in situ* Auger spectrometer (LK Technologies) and it was found that the perovskite substrates are deteriorated by photodissociated chlorine. Hence, after each photochemistry cycle the surface was cleaned by 10 minutes sputtering at 300 K (Ne^+ ions at 600 V and a sample current of ~2 μA).

2.4 Luminescence studies

Electron beam-induced luminescence (EBIL) studies were performed at temperatures (of the perovskite samples) between 40 K and 300 K using a 2000 eV electron beam (Kimball Physics, ELG-2) as the e-beam excitation source. Photoluminescence (PL) studies were performed following 355 nm laser irradiation (third harmonic of a Nd:YAG laser at the power of 1 mJ cm^{-2} per pulse) as the light excitation source. Both photon- and electron-induced luminescence signals were measured using an Ocean Optics spectrometer (USB2000+ model) from outside of the UHV chamber through the optical viewing port.

3. Results and discussion

3.1 Adsorption of EC on the halide perovskite surfaces

Before reporting on the photochemistry of EC on $CsPbBr_3$ and $MAPbBr_3$, we briefly describe the thermal adsorption and desorption of EC from these halide perovskite substrates, since such experiments have not been reported previously. TPD experiments of the parent EC molecule (detected at mass 29) from clean SiO_2/Si(100) reveal a single desorption peak at 85 K, whereas experiments under similar conditions performed on $CsPbBr_3$ and $MAPbBr_3$ perovskite-covered surfaces reveal two desorption peaks around 92–110 K. From the TPD results performed with different EC exposures shown in Fig. 1 and Fig. S3 (ESI†), we estimated that an exposure of 1.5 Langmuirs

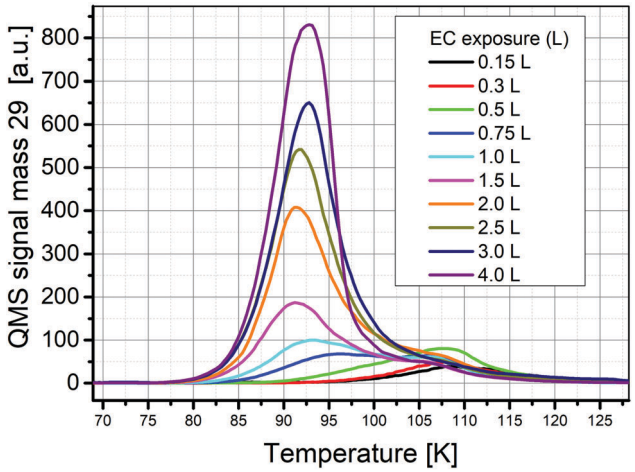

Fig. 1 Temperature programmed desorption (TPD) of ethyl chloride from a halide perovskite substrate: TPD spectra of EC from a 400 nm thick $CsPbBr_3$ film deposited on a SiO_2/Si(100) sample at the indicated exposures in Langmuirs (L) (1 L = 10^{-6} Torr s). Exposure values were corrected for the ion gauge sensitivity factor. Heating rates were 1 K s^{-1}.

(L) EC (1 L = 10^{-6} Torr s) leads to 1 ML (monolayer) EC coverage on both halide perovskite substrates (implying an identical sticking probability of EC on both substrates). These results were confirmed by electron-induced luminescence (EBIL) studies (Fig. S7, ESI†). Assuming a pre-exponential factor of 10^{13} Hz (for first order desorption kinetics), the binding energies of an EC molecule on the halide perovskite surfaces (detected *via* mass 29 using TPD line shape analysis) were estimated to be 5.6 ± 0.5 kcal mol^{-1} and 6.2 ± 0.5 kcal mol^{-1} for $CsPbBr_3$ and $MAPbBr_3$, respectively. This suggests that the interaction between ethylchloride and perovskite is physisorption in nature.

3.2 Photodissocation of EC on the halide perovskite substrates

The photochemical activity of the halide perovskite materials was studied by monitoring the photo-dissociation of EC molecules adsorbed on both $CsPbBr_3$ and $MAPbBr_3$ surfaces, by employing TPD measurements following visible light irradiation. Several masses were recorded simultaneously, including the parent molecule and the most abundant photoproducts as a function of the number of photons striking the halide perovskite surfaces. Specifically, ethane (Mass-30, C_2H_6), the allyl radical (Mass-41, C_3H_5) and the propyl radical (Mass-43, C_3H_7) were monitored. Post-irradiation TPD spectra of these most abundant photoproducts were obtained following visible light laser (6 ns pulse duration at 532 nm) excitation of 1 ML EC adsorbed on the perovskite samples as a function of the number of photons (or laser pulses) striking the surface (Fig. 2 and Fig. S4 in ESI†). These spectra indicate that the parent molecule population depletes as the number of pulses grows from 0 to 2.7 × 10^{18} photons, with a simultaneous increase in the population (coverage) of the photoproducts. Ethane desorbs *via* a sharp peak at 40 K and 45 K from $MAPbBr_3$ and $CsPbBr_3$ respectively, whereas the allyl and the propyl radicals desorb at 65–100 K and 50–100 K, respectively. As can be seen, propyl radicals exhibit similar TPD spectra to the allyl radicals

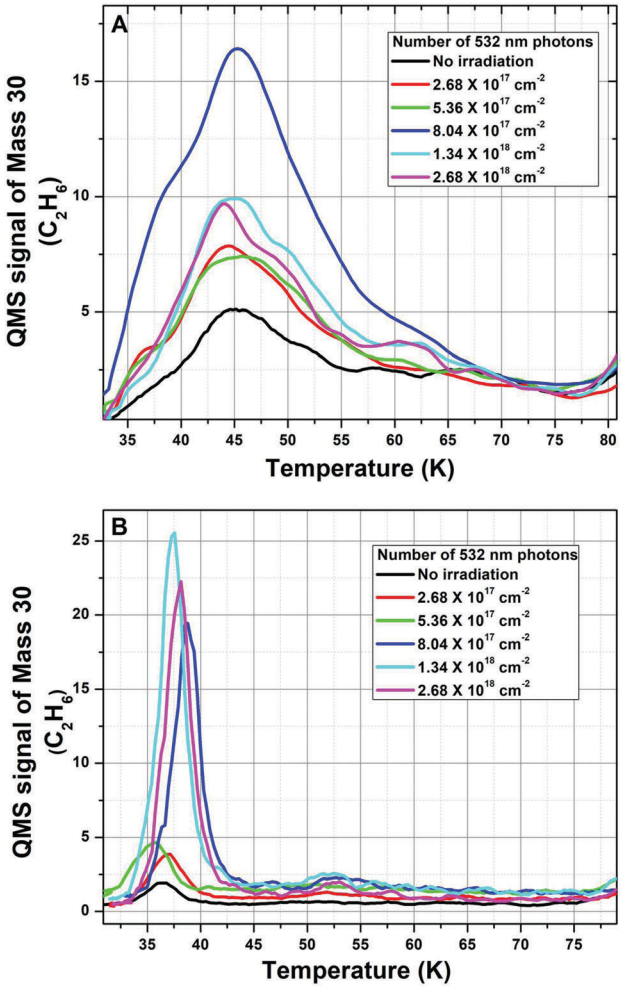

Fig. 2 Post-irradiation TPD spectra of the photogenerated product, ethane (Mass 30, C_2H_6) at the indicated number of 532 nm photons striking the sample (A) $CsPbBr_3$ and (B) $MAPbBr_3$. The heating rate was 1 K s^{-1}.

(Fig. S4 in ESI†), suggesting that both of them originate from the same precursor parent molecule butane (Mass 58, C_4H_{10}) as a result of fragmentation within the QMS.[18] In both of the perovskites, the ratio between propyl and allyl radicals was ~1 : 1 (taken from the experiment in which maximum photochemical yield is observed). This ratio is less than the reported literature value (3 : 1) [18] suggesting the presence of butene (Mass 56, C_4H_8) as another possible photochemical product, contributing its fragments to the allyl radical.

In Fig. 3 and in Fig. S5 in the ESI,† we compare the integrated area under the TPD spectra of these most abundant photoproducts (normalized to that of the parent EC molecule without irradiation). The yield of the photoproducts increases with increasing number of photons, and eventually reaches saturation. The saturation is observed when the number of photons striking the surface is > 8.0 × 10^{17} photons in the case of $CsPbBr_3$ and > 1.3 × 10^{18} photons for $MAPbBr_3$. As shown in Fig. 3, the increasing ethane coverage was fitted with an exponential saturation curve and the cross section values were found to be 4.5 ± 0.2 × 10^{-18} cm^2

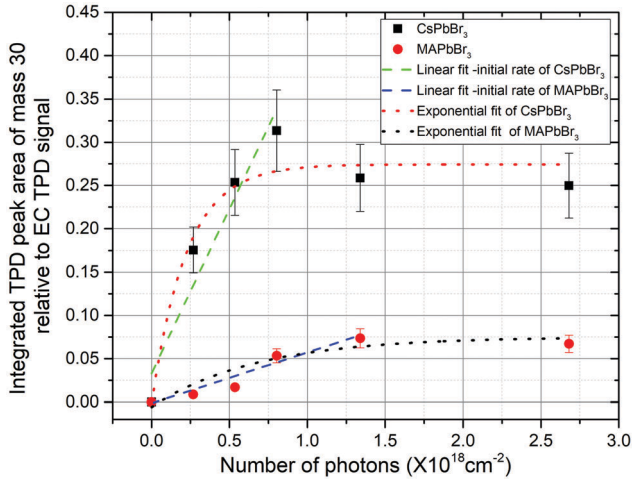

Fig. 3 Integrated TPD peaks *vs.* visible (532 nm) light excitation of the photgenerated product ethane (Mass 30, C_2H_6), (derived from Fig. 2) *vs.* the number of 532 nm photons striking the $CsPbBr_3$ and $MAPbBr_3$ perovskite samples. Exponential fit (red and black) and linear fit for the initial growth (green and blue) were used to demonstrate how cross sections of the formation of product molecules were determined.

and $1.5 \pm 0.8 \times 10^{-19}$ cm^2 for $CsPbBr_3$ and $MAPbBr_3$, respectively. In contrast, the cross section values obtained using linear fits of the initial formation rates were smaller, *viz.* $3.8 \pm 0.7 \times 10^{-19}$ cm^2 for $CsPbBr_3$ and $5.8 \pm 0.7 \times 10^{-20}$ cm^2 for $MAPbBr_3$. This discrepancy can be explained by surface poisoning, induced by adsorption of chlorine atoms dissociated from EC. This was also confirmed by an increased Cl signal observed in Auger spectra taken following the photochemistry runs (Fig. 4). Therefore, due to poisoning and saturation at higher photon doses, the initial formation rates of photo products (ethane, propyl and allyl radicals) were used to derive the more accurate cross sections for EC photo-dissociation. From the linear fitting of the initial photo product growth, the cross sections for ethane, propyl and allyl radical formation were derived (see Fig. S4 and S5 in ESI†) and the values are given in Table 1. Almost identical cross sections obtained for the formation of the allyl and the propyl radicals indicate that both originate from the same precursor molecule – butane.

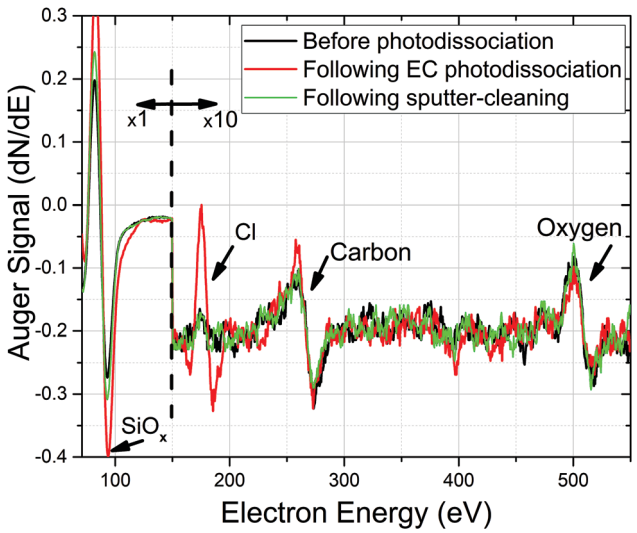

Fig. 4 Auger spectra of EC on top of $CsPbBr_3$, before photo-dissociation (black), following EC photo fragmentation (red) and after cleaning the surface of $CsPbBr_3$ by sputtering (green).

From the cross section values, it is clear that photo-reactivity on top of the $CsPbBr_3$ surface is an order of magnitude more effective than on the $CH_3NH_3PbBr_3$. This correlates well with the stronger PL intensity, reflecting the low density of surface defects.

3.3 Luminescence

The objective of studying photoluminescence (PL) and electron beam-induced luminescence (EBIL) was their potential as guiding tools for the presence of surface states and defects. Fig. 5 illustrates the temperature-dependent EBIL spectra of $CsPbBr_3$ recorded from 35 to 150 K. At 35 K an emission peak located at 2.31 eV (537 nm) is observed, displaying a systematic blue-shift when the temperature increases from 40 to 150 K. PL spectra were measured as well, revealing a similar blue shift at low temperature, while in the high temperature range (from 180 to 300 K), the peak position does not change anymore (see Fig. S6 in ESI†). In the case of the PL spectra taken from $CsPbBr_3$, a single and relatively narrow peak is recorded in the entire temperature range, which can be attributed to the emission from the lowest state exciton only, indicating negligible trap state density. In contrast, from $MAPbBr_3$, in addition to lower PL intensity, there is a split into two peaks at 120 K which can be attributed to the presence of surface states (see Fig. S6 in ESI† and further discussion therein).

Interestingly, the EBIL intensity is found to be about five times brighter than the PL intensity. The flux of impinging electrons (1 μA = 6.3×10^{12} electron per s) on the $CsPbBr_3$ substrate is four orders of magnitude smaller than that of the photons (the number of photons per s at 355 nm laser irradiation is 1.8×10^{16} s^{-1}) used for the PL studies. Hence the overall cross section for electron induced luminescence at 2 keV is more than four orders of magnitude larger than that of photo-induced luminescence. In addition, the EBIL signal is much more strongly quenched with increasing temperature than the PL one. The signal diminished by almost half when the temperature increased from 40 to 50 K and it completely vanished above 150 K, apparently

Table 1 Formation cross sections for photoproducts (ethane, allyl radical, propyl radical) following photon irradiation at 532 nm of EC adsorbed on top of the two indicated perovskite surfaces

	Cross section value (σ)		
Perovskite substrate	Ethane (Mass 30) (Mass 30, C_2H_6)	Allyl radical (Mass 41, C_3H_5)	Propyl radical (Mass 43, C_3H_7)
$CsPbBr_3$	$6.9 \pm 0.1 \times 10^{-19}$ cm^2	$1.7 \pm 0.3 \times 10^{-19}$ cm^2	$1.8 \pm 0.1 \times 10^{-19}$ cm^2
$MAPbBr_3$	$6.0 \pm 0.1 \times 10^{-20}$ cm^2	$1.8 \pm 0.1 \times 10^{-20}$ cm^2	$2.0 \pm 0.4 \times 10^{-20}$ cm^2

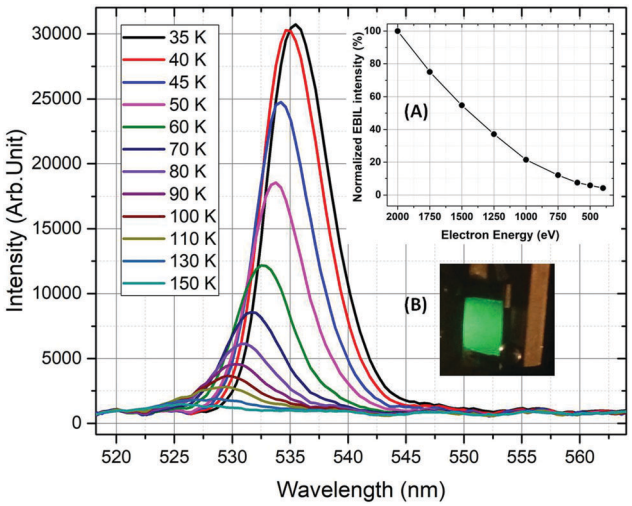

Fig. 5 Electron beam induced luminescence (EBIL) of $CsPbBr_3$, excited by a 2 keV electron beam. Inset (A) shows the electron beam-induced luminescence (EBIL) of $CsPbBr_3$ as a function of excitation e-beam energy and (B) shows the photograph of $CsPbBr_3$ illuminated with the e-beam.

due to strong electron–phonon coupling.[19,20] Furthermore, the luminescence signal is stable for a long time (tens of minutes) while the same spot on the sample was being excited by the electron beam. Improved stability of the $CsPbBr_3$ film during irradiation by photons or electrons over the $MAPbBr_3$ one has previously been reported;[21] the present results provide vivid evidence for the effect of ambient atmosphere on (in)stability. Although the high energy spectroscopy (2 keV, a typical core energy excitation range used in *e.g.* Auger spectroscopy) of these perovskites is unknown with respect to luminescence excitation, it seems that the EBIL excitation is a significantly higher probability process than the 355 nm optical excitation, even though both end up populating the same emitting low energy state. In addition, the fact that EBIL disappears if the electron energy drops below 500 eV (see inset A of Fig. 5) suggests that the energetic window for the EBIL method is limited to electron energy >500 eV. Attempts to obtain similar EBIL data from $MAPbBr_3$ samples was unsuccessful, probably due to e-beam damage of the organic part (methylamine) of the material (as CH_3NH_2 can escape as gas, in contrast to Cs). This is consistent with our EBIC studies[21] where the two materials were compared using 3 keV electrons and $MAPbBr_3$ was found to be less stable under the e-beam irradiation.

We conclude that the photochemistry data are consistent with the luminescence results. Higher photo-reactivity on top of the $CsPbBr_3$ surface can be attributed to the low density of defects as implied from the EBIL and photoluminescence studies.

4. Conclusions

The photochemical activity of $CsPbBr_3$ (inorganic) and $MAPbBr_3$ (organic) halide perovskites under visible light irradiation has been studied *via* photo-fragmentation of ethyl chloride (EC) using a nanosecond pulsed visible light (532 nm) laser excitation procedure for the first time. Post-irradiation TPD experiments and *in situ* Auger electron spectroscopy indicate that the C–Cl bond dissociates following the visible light excitation to form surface-bound Cl atoms, ethane, and butane. Previous studies under similar conditions with EC on top of SiO_2/Si(100) or on silver nanoclusters on SiO_2/Si(100) surfaces found no photo-reactivity whatsoever upon irradiation at 532 nm.[17] Among the two perovskites, $CsPbBr_3$ exhibits an order of magnitude higher photochemical cross section than $MAPbBr_3$ to decompose the probe EC molecule. Moreover, compared to typical photochemical cross sections on, *e.g.* silver substrates (10^{-21}–10^{-20} cm^2), the perovskites reveal about an order of magnitude higher photo-reactivity. If these halide perovskites are protected against damage due to water and oxygen, the observations reported here provide a good basis to explore their use for other photo-catalytic applications such as water splitting.

These observations support our conclusion that a correlation exists between bright electron- or photon-induced luminescence, efficient photovoltaic performance and photo-reactivity in the visible optical range, as reported in this work.

Author contributions

SH, SR and MA are responsible for the entire photochemistry and luminescence studies under UHV conditions. MK, IL and DC are responsible for the $CsPbBr_3$ sample preparation. B.-E. C and L. E. are responsible for the $MAPbBr_3$ sample preparation.

Conflicts of interest

The authors declare no competing financial interests.

Acknowledgements

MA acknowledges the partial financial support of the Israel Science Foundation (ISF) and the Einstein Foundation Berlin. LE acknowledges the partial support by the Israeli Ministry of Science under China-Israel program and the Einstein Foundation Berlin. DC acknowledges the partial support provided by the EraNet project and the Ullman Family Foundation.

References

1 A. Landman, H. Dotan, G. E. Shter, M. Wullenkord, A. Houaijia, A. Maljusch, G. S. Grader and A. Rothschild, Photoelectrochemical water splitting in separate oxygen and hydrogen cells, *Nat. Mater.*, 2017, **16**, 646.
2 I. K. Konstantinou and T. A. Albanis, TiO_2-assisted photocatalytic degradation of azo dyes in aqueous solution: kinetic and mechanistic investigations: a review, *Appl. Catal., B*, 2004, **49**, 1–14.
3 T. Kamegawa, Y. Shimizu and H. Yamashita, Superhydrophobic Surfaces with Photocatalytic Self-Cleaning Properties by Nanocomposite Coating of TiO_2 and Polytetrafluoroethylene, *Adv. Mater.*, 2012, **24**, 3697–3700.

4 D. Li, H. Haneda, S. Hishita and N. Ohashi, Visible-light-driven N-F-codoped TiO_2 photocatalysts. 2. Optical characterization, photocatalysis, and potential application to air purification, *Chem. Mater.*, 2005, **17**, 2596–2602.
5 O. K. Varghese, M. Paulose, T. J. LaTempa and C. A. Grimes, High-Rate Solar Photocatalytic Conversion of CO_2 and Water Vapor to Hydrocarbon Fuels, *Nano Lett.*, 2009, **9**, 731–737.
6 S. Kazim, M. K. Nazeeruddin, M. Grätzel and S. Ahmad, Perovskite as Light Harvester: A Game Changer in Photovoltaics, *Angew. Chem., Int. Ed.*, 2014, **53**, 2812–2824.
7 N.-G. Park, Organometal Perovskite Light Absorbers Toward a 20% Efficiency Low-Cost Solid-State Mesoscopic Solar Cell, *J. Phys. Chem. Lett.*, 2013, **4**, 2423–2429.
8 W. Li, Z. Wang, F. Deschler, S. Gao, R. H. Friend and A. K. Cheetham, Chemically diverse and multifunctional hybrid organic–inorganic perovskites, *Nat. Rev. Mater.*, 2017, **2**, 16099.
9 M. Kulbak, D. Cahen and G. Hodes, How Important Is the Organic Part of Lead Halide Perovskite Photovoltaic Cells? Efficient $CsPbBr_3$ Cells, *J. Phys. Chem. Lett.*, 2015, **6**, 2452–2456.
10 C. R. Kagan, D. B. Mitzi and C. D. Dimitrakopoulos, Organic-Inorganic Hybrid Materials as Semiconducting Channels in Thin-Film Field-Effect Transistors, *Science*, 1999, **286**, 945.
11 G. Xing, N. Mathews, S. S. Lim, N. Yantara, X. Liu, D. Sabba, M. Grätzel, S. Mhaisalkar and T. C. Sum, Low-temperature solution-processed wavelength-tunable perovskites for lasing, *Nat. Mater.*, 2014, **13**, 476.
12 H. Sun, T. Lei, W. Tian, F. Cao, J. Xiong and L. Li, Self-Powered, Flexible, and Solution-Processable Perovskite Photodetector Based on Low-Cost Carbon Cloth, *Small*, 2017, **13**, 1701042.
13 https://www.nrel.gov/pv/assets/images/efficiency-chart.png.
14 P. Zhang, T. Ochi, M. Fujitsuka, Y. Kobori, T. Majima and T. Tachikawa, Mesocrystal Superstructures with Anisotropic Construction for Efficient Overall Water Splitting, *Angew. Chem., Int. Ed.*, 2017, **56**, 5299–5303.
15 Y. Cui, J. Briscoe and S. Dunn, Effect of Ferroelectricity on Solar-Light-Driven Photocatalytic Activity of $BaTiO_3$—Influence on the Carrier Separation and Stern Layer Formation, *Chem. Mater.*, 2013, **25**, 4215–4223.
16 T. Alammar, I. Hamm, V. Grasmik, M. Wark and A.-V. Mudring, Microwave-Assisted Synthesis of Perovskite $SrSnO_3$ Nanocrystals in Ionic Liquids for Photocatalytic Applications, *Inorg. Chem.*, 2017, **56**, 6920–6932.
17 G. Toker, A. Bespaly, L. Zilberberg and M. Asscher, Enhanced Photochemistry of Ethyl Chloride on Ag Nanoparticles, *Nano Lett.*, 2015, **15**, 936–942.
18 S. E. Stein, Mass Spectra. In NIST Chemistry WebBook, P.J. Linstrom, W. G. Mallard, ds., National Institute of Standards and Technology: Gaithersburg, MD; NIST Standard Reference Database Number 69, 20899, http://webbook.nist.gov.
19 K. Wei, Z. Xu, R. Chen, X. Zheng, X. Cheng and T. Jiang, Temperature-dependent excitonic photoluminescence excited by two-photon absorption in perovskite $CsPbBr_3$ quantum dots, *Opt. Lett.*, 2016, **41**, 3821–3824.
20 D. Zhang, S. W. Eaton, Y. Yu, L. Dou and P. Yang, Solution-Phase Synthesis of Cesium Lead Halide Perovskite Nanowires, *J. Am. Chem. Soc.*, 2015, **137**, 9230–9233.
21 M. Kulbak, S. Gupta, N. Kedem, I. Levine, T. Bendikov, G. Hodes and D. Cahen, Cesium Enhances Long-Term Stability of Lead Bromide Perovskite-Based Solar Cells, *J. Phys. Chem. Lett.*, 2016, **7**(1), 167–172.

